PEER REVIEWED

Superhydrophobic Surface on Arc-Sprayed Aluminum Coating Via Fluorinated Polyurethane Modification: Preparation and Application in Corrosion Protection

Ning Li[1,2,3] · Ye Tian[2,3] · Rui Yang[2,3] · Haijun Zhang[2,3] · Hua Li[1,2,3] · Xiuyong Chen[2,3,4]

Abstract This study aimed to prepare a superhydrophobic coating by applying low surface energy (LSE) materials to a rough surface, intending to achieve a corrosion-resistant coating. Polyurethane (PU) and fluorinated polyurethane (FPU) were synthesized via designed routes as LSE materials. Arc-sprayed aluminum (Al) coatings and 316L stainless steel substrates (316L SS) were used as the rough and smooth surfaces, respectively. The synthesized PU/FPU coatings were formed on the Al coatings and 316L SS, and their hydrophobicity and corrosion resistance were evaluated. The water contact angle test showed that the content of the fluorine and the concentration of the PU/FPU could affect the hydrophobicity of the surface. In addition, superhydrophobicity was achieved via applying FPU to a rough Al coating surface (Al-FPU coating). Furthermore, the Al-FPU coating also exhibited better corrosion resistance than that of the PU and the pure Al coatings according to Tafel polarization curves and electrochemical impedance spectra in artificial seawater. The results suggested that surface energy and surface roughness were correlated with hydrophobicity, and the modification via fluorinating can be an effective method to achieve superhydrophobicity and corrosion resistance for thermal-sprayed coatings.

Introduction

Metal corrosion is especially grave in engineering fields such as ships, automobiles, pipelines and aircraft, both financially and operationally (Ref 1). The hydrophobic surfaces offer enormous possibilities for corrosion protection of metals and alloys. Superhydrophobic surfaces with water contact angle (WCA) greater than 150° and sliding angle (SA) lower than 10° have a wide range of applications in waterproof, antifouling, corrosion protection, antibacterial and other fields (Ref 2, 3) due to its unique physical and chemical properties, such as self-cleaning (Ref 4, 5), antifouling (Ref 6), anti-corrosion (Ref 7), anti-icing (Ref 8, 9) and resistance reduction (Ref 10). Material with low surface energy (LSE) is conducive to achieving surface hydrophobicity. However, the maximum water contact angle can only reach 120° on the smooth surface treated with LSE materials (Ref 11), which is far below the requirements of superhydrophobicity. Therefore, the current research is primarily concerned with improving the surface roughness to achieve a superhydrophobic surface, which can be accessed in two ways: either applying a layer of LSE materials on the rough surface or roughening the

✉ Xiuyong Chen
chenxiuyong@nimte.ac.cn

1 Henan Institute of Advanced Technology, Zhengzhou University, Zhengzhou 450052, China

2 Key Laboratory of Marine Materials and Related Technologies, Zhejiang Key Laboratory of Marine Materials and Protective Technologies, Ningbo Institute of Materials Technology and Engineering, Chinese Academy of Sciences, Ningbo 315201, China

3 Zhejiang Engineering Research Center for Biomedical Materials, Cixi Institute of Biomedical Engineering, Ningbo Institute of Materials Technology and Engineering, Chinese Academy of Sciences, Ningbo 315201, China

4 Center of Materials Science and Optoelectronics Engineering, University of Chinese Academy of Sciences, Beijing 100049, China

surface of LSE materials. In other words, a superhydrophobic surface can be produced by combining LSE materials with a rough surface. Generally, fluoropolymers (Ref 12, 13) and silicone polymers (Ref 14-16) are the typical LSE materials, as the C-F bond in fluoropolymers and the Si-O bond in silicone polymers have higher bond energy. Meanwhile, rough structures can be constructed by anode oxidation (Ref 17), electrochemical deposition (Ref 18), photochemical (Ref 19), sol–gel (Ref 20), vapor deposition (Ref 21), electrostatic spinning (Ref 22) and layer self-assembly (Ref 23). Nevertheless, these approaches are highly technically demanding, and thus, long-cycle, large-scale and low-cost preparation methods remain the key to the applications.

Thermal-sprayed Al coatings are also extensively adopted for corrosion protection (Ref 24-26). However, the service life of the thermal-sprayed Al coatings can be reduced by the porosity which is generally existed in the actual as-sprayed coatings (Ref 27, 28). Hence, polymer sealants are widely used to address the problem (Ref 29-31), and applying the polymer sealants with LSE to the thermal-sprayed Al coating may further improve the corrosion resistance via hydrophobicity. Meanwhile, the thermal spray technique can deposit Al coatings with certain roughness (Ref 32), which is also necessary to achieve superhydrophobicity. Thus, combining the thermal spray technique and the LSE materials may provide the coatings with very effective corrosion resistance by achieving superhydrophobicity (Ref 33). Recently, different thermal spray methods have been developed for depositing various engineering materials on various substrates, thereby making it possible to prepare large-scale superhydrophobic coatings (Ref 34, 35). Therefore, it is worthwhile to further develop superhydrophobic coatings via thermal spray deposition and following additional surface modification.

In this study, arc-sprayed Al coatings were deposited on 316L stainless steel (316L SS) substrates, which provide rough surfaces. Since fluoropolymers exhibit LSE, a series of polyurethane (PU) materials with increasing fluorine contents were synthesized and then applied to the Al coatings. The superhydrophobic properties of the Al coatings modified by the fluorinated polyurethanes (FPU) with different fluorine contents were investigated. Meanwhile, the effect of the Al coating thickness on hydrophobicity was also performed. Furthermore, the effects of PU/FPU modifications on the corrosion protection of the Al coatings were studied.

Experimental Procedure

Vinylidene fluoride-hexafluoro propene copolymer (VDF-co-HFP, FKM2601, Zhonghao Chenguang Research Institute of Chemical Industry, China) with VDF/HFP = 3/1 and a number average molecular weight (M_n) of 116107 was used as the fluorine source. Hydrogen peroxide (H_2O_2), potassium hydroxide (KOH), hydrochloric acid (HCl), tetrahydrofuran (THF) and acetone were obtained from Sinopharm Chemical Reagent, China. Benzyl triethyl ammonium chloride (BTEAC), lithium aluminum hydride ($LiAlH_4$), ethyl acetate (EA), N,N-dimethylformamide (DMF) and poly-tetrahydrofuran glycol (PTMG, Mn=1000) were purchased from Aladdin Chemistry Co., China. 4,4-diphenylmethane diisocyanate (MDI) was purchased from Alfa Aesar Co., China. Al wire (Φ2 mm, Beijing General Research Institute of Mining & Metallurgy, China) was used for arc spraying to form a rough surface on 316L SS substrate (Zechanglong Ltd., China).

Hydroxyl-terminated liquid fluoropolymer (LFH) was synthesized according to Formula 1 & 2 (Scheme 1). After that, a viscous buff liquid (LFH contained) was obtained, whose mass average molecular weight (M_w) was 1831 and polydispersity index (PDI) was 1.21. FPUs were prepared via a two-step method. Formula 3 (Scheme 1) shows the synthesis process of the fluorinated polyurethane prepolymer (PreFPU). In this study, PU and six kinds of FPU with different dosages of LFH (FPU-5, FPU-10, FPU-15, FPU-20, FPU-25 and FPU-30) were successfully synthesized, and the dosages of LFH were 5 wt.%, 10 wt.%, 15 wt.%, 20 wt.%, 25 wt.% and 30 wt.%, respectively. The prepared PreFPU was dissolved in N,N-dimethylformamide (DMF) in a ratio of 1: 3. The solution was directly dripped onto a clean glass surface, naturally leveled and then dried at 60 °C. This process was repeated five times, and then, an FPU film with a thickness of 0.5 mm was obtained.

The FPU coating was formed on the 316L SS substrates and the arc-sprayed Al coatings. The specific steps to prepare the Al coating using arc spraying were as follows. The 316L SS was machined into 20 × 20 × 2 mm. The machined 316L SS substrates were then ultrasonic cleaned by ethanol and dried. The cleaned 316L SS substrates were sandblasted by alumina (240-300 grit) at 0.7 MPa. After sandblasting, the substrates were blown by compressed air to remove the remaining sand particles on the surfaces. Next, the Al coatings were deposited to the substrates via arc spraying (EuTronic Arc Spray 4 HF, Castolin-Eutectic Pte Ltd., USA). The spraying parameters are shown in Table 1. During the spraying process, the number of the spray passes was controlled to deposit Al coatings with different thicknesses. Finally, the 316L SS substrates and the Al coatings were immersed in the solutions with PU or FPU-20 concentrations of 0.5 wt.%, 1.0 wt.%, 1.5 wt.%, 2.0 wt.%, 2.5 wt.%, 5.0 wt.% and 10.0 wt.% for 10 minutes and dried at room temperature.

Attenuated total reflection Fourier transform infrared spectroscopy (ATR-FTIR) measurement was taken using an infrared spectrometer (Nicolet iS50, Thermo Scientific,
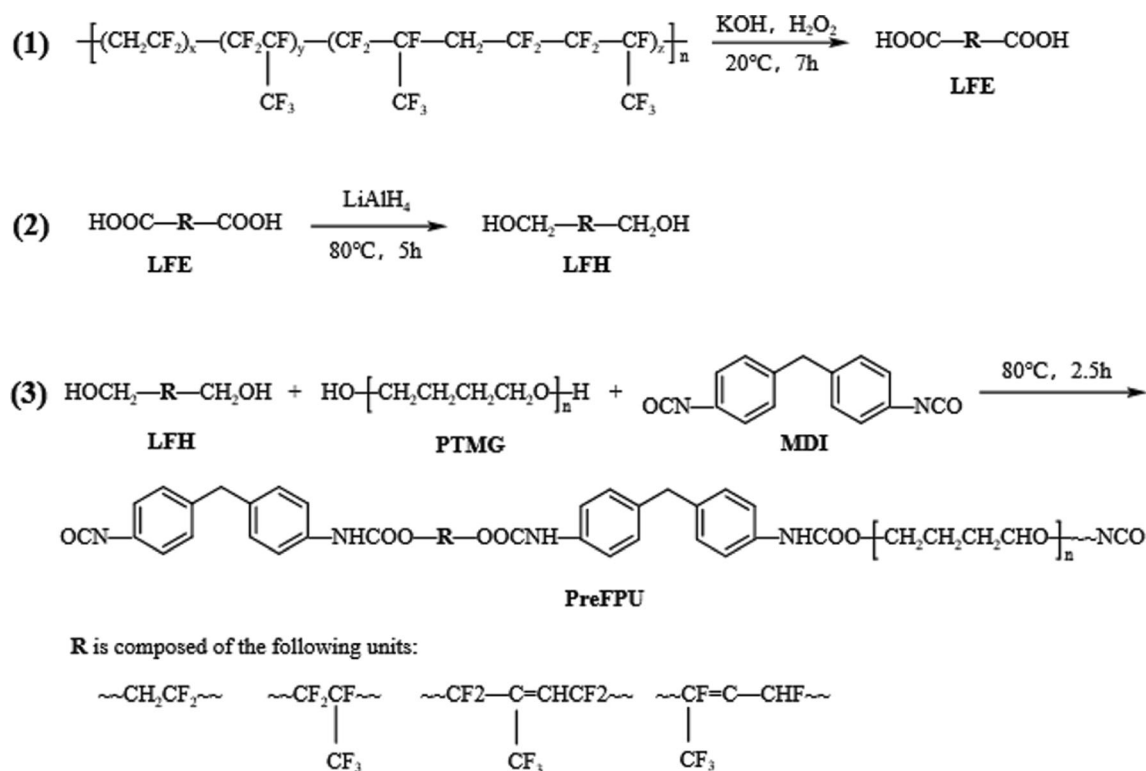
Scheme 1 Designed routes for the synthesis of fluorinated polyurethane. Formula (1), carboxyl-terminated liquid fluoropolymer (LFE); Formula (2), hydroxyl-terminated liquid fluoropolymer (LFH); Formula (3), fluorinated polyurethane prepolymer (PreFPU)

Table 1 Process parameters of arc spraying

Current	Voltage	Distance	Compressed air
100 A	25 V	150 mm	0.5 MPa

America). The spectra were recorded in 400-4000 cm^{-1} at a 4 cm^{-1} resolution. M_w and PDI of the polymers were obtained by gel permeation chromatography (GPC) system (PL-GPC 220, Agilent Technologies Inc., USA). THF was used as a solvent with a flow rate of 1 ml/min at 30 °C. The content of carboxyl groups was characterized by automatic potentiometric titration (Tiamo 905, Metrohm, Switzerland) with acetone as the solvent. Glass electrode and calomel electrode were used as the indicator and the reference electrodes, respectively. The ^{1}H and ^{19}F spectra were analyzed by a nuclear magnetic resonance spectrometer (NMR, AVANCE III 400MHz, Bruker, Switzerland) using acetone-*d6* as solvent.

WCA measurement was taken using a goniometer (DSA 25, KRUSS, Germany). The volume of the deionized water for the static contact angle tests is 4 μL, and the volume of the deionized water for the sliding angle tests is 10 μL. Three samples were tested for each type, and three sites were evaluated for each sample. The surface profile and surface roughness were measured by a 3D optical profilometer (UP-Lambda, Rtec Instruments, USA). The roughness (R_a) of the FPU films was firstly quantified via the root-mean-square (rms) roughness acquired by white light interferometry. Scanning electron microscopy (SEM, Regulus 8230, HITACHI, Japan) was used to analyze the surface morphology.

The electrochemical data of the coatings in artificial seawater solution were measured via the electrochemical workstation (CHI660E, Shanghai Chenhua Co., Ltd, China). The counter electrode (CE) was platinum, the reference electrode (RE) was saturated calomel, and the working electrode (WE) was a sample with a working area of 10×10 mm^2. Firstly, the sample was immersed in artificial seawater for 2 h to obtain a stable open circuit potential (E_{ocp}). For the electrochemical impedance spectroscopy (EIS) test, the frequency range was 10^5 to 10^{-2} Hz, and the amplitude was 10 mV. The EIS data were fitted and analyzed by ZSimDemo software. For the potentiodynamic polarization curves test, the range of potential was -1.3 to 0.1 V at a scanning rate of 1 mV/s, and the sensitivity was 1 mA/V. The acquired data were analyzed by the CHI660E software.

A 15-day (360 h) salt spray test (Q-FOG CCT1100 salt spray test chamber, Q-LAB Co., Ltd, USA) was performed to evaluate the corrosion resistance of the coating as per

ASTM B117-2007. The concentration of the NaCl in the solution was 5 %, and the pH was controlled in a range of 6.5 ~ 7.2. The spraying pressure was 1 kg/cm^2, and the humidity was maintained above 95%. The temperature of the chamber was held at 35 °C. The non-coated side and the edges of the samples were sealed. During the test, the samples were placed at 15° to the horizontal in the chamber and photographed every 24 h.

Results and Discussion

The ^{1}H and ^{19}F spectroscopy analyses show the structures of the LFH and the precursor LFE. As shown in Fig. 1a, compared to the precursor, the peaks at 7.57 ppm and 7.65 ppm disappeared, and LFH showed a new peak at 3.77 ppm, proving that –COOH was restored to –CH$_2$OH. Furthermore, the peaks at 4.69 ppm, 2.85 to 3.51 ppm and 1.55 ppm were ascribed to –C(CF$_3$) =CH–, –CH$_2$CF$_2$– and –CHF–C(CF$_3$) =CF–, respectively (Ref 36, 37). The ^{19}F NMR spectra of the LFE and LFH can be found in Fig. 1b. For the LFE, the peak at −63.66 ppm ascribes to –CF$_2$-COOH. The curve of the LFH exhibited a new peak at −105.81 ppm, which was ascribed to the chemical shift of

Fig. 1 NMR spectra of the LFH and its precursor LFE in acetone-d_6. (a), ^{1}H NMR spectra; (b), ^{19}F NMR spectra

the F atom in –CF$_2$CH$_2$OH (Ref 38). The NMR spectra evidenced the successful synthesis of the LFH.

The FTIR spectrum of LFH is shown in Fig. 2a. Meanwhile, the spectra of the LFE and the raw material (VDF-co-HFP) are also presented in the figure as comparisons. All the materials exhibited the same absorption peaks at 1397, 1178 and 880 cm^{-1} ascribed to the stretching vibration of –FCH$_2$–, –CF$_2$– and –CF$_3$, which showed that they had the same backbone structure (Ref 37). The new peak of the LFE at 1756 cm^{-1} is ascribed to the stretching vibration of C=O, suggesting the formation of –CF$_2$COOH. Compared with the precursor LFE, the LFH exhibited a new peak at 3330 cm^{-1} attributed to the stretching vibration of –OH, and the peak of C=O disappeared. The new peak at 3330 cm^{-1} and the absence of the C=O peak evidenced that LFH was successfully prepared from large molecular weight VDF-co-HFP by oxidative degradation and reduction reaction.

The FTIR spectra of the MDI, PTMG, LFH, PreFPU and FPU are displayed in Fig. 2b. Compared with the PreFPU and MDI, the FPU exhibited a new peak at 3320 cm^{-1}, which was attributed to the stretching vibration of N-H. Moreover, the peak of -NCO at 2262 cm^{-1} was absent in the FPU, indicating the reactant MDI had been completely consumed. In addition, all the materials exhibited the same absorption peaks at 1397, 1178 and 880 cm^{-1} ascribed to stretching vibration of -FCH$_2$-, -CF$_2$- and -CF$_3$, which suggested that they had the same backbone structure (Ref 39). Hence, the FTIR spectra confirmed that the synthesis of fluorinated polyurethane (FPU) was successful.

The PU and the FPU with different dosages of LFH were prepared on a glass surface (substrate) to study the effect of the fluorine content on the surface roughness (R_a) and hydrophobicity of PU. Figure 3 demonstrates the relationship of R_a and WCA of the glass substrate, the PU and the FPU with different dosages of LFH. The glass substrate exhibited hydrophilicity with a WCA of 41.6±0.7°, and the surface of the glass substrate was very smooth with the R_a of 0.89±0.11 nm. The results demonstrate that with the increase in the LFH content, the R_a and WCA tended to increase at a low dosage of LFH, but decrease at a high dosage. The results show that pure PU had the lowest R_a of 0.30 μm and a WCA of 81.2±3.8°. When the dosage of LFH was increased to 15 wt.%, the R_a of the FPU film reached a maximum of 3.96 μm, and the WCA was 110.3±1.3°. As the dosage of LFH continued to increase, R_a started to decrease, but the WCA still increased to 112.5±1.7° and then decreased. This result suggests that the fluoric group could effectively improve the hydrophobicity of the fluorinated polyurethane. That is due to the LSE by the high electronegativity and polarity of the fluorine atoms. However, when the dosage of LFH reached a critical value, the R_a of the FPU films started to
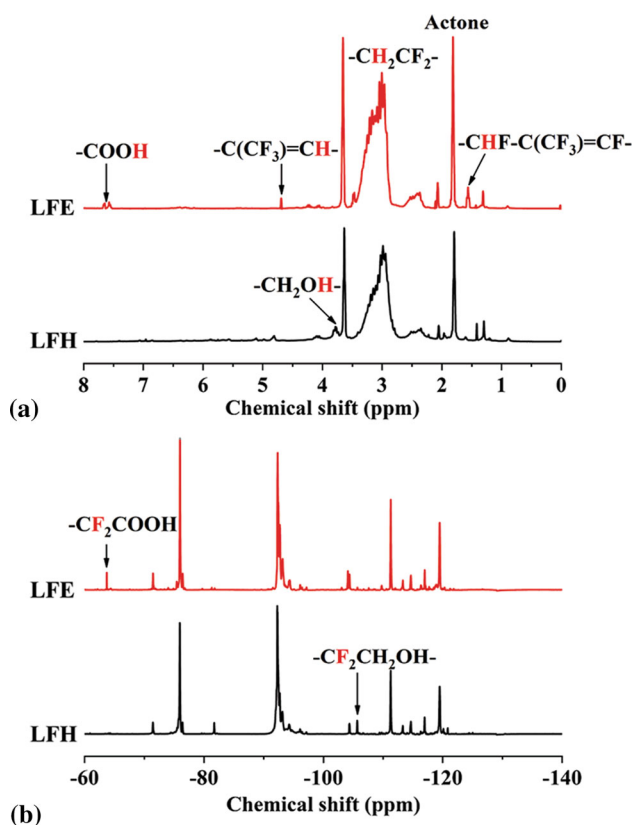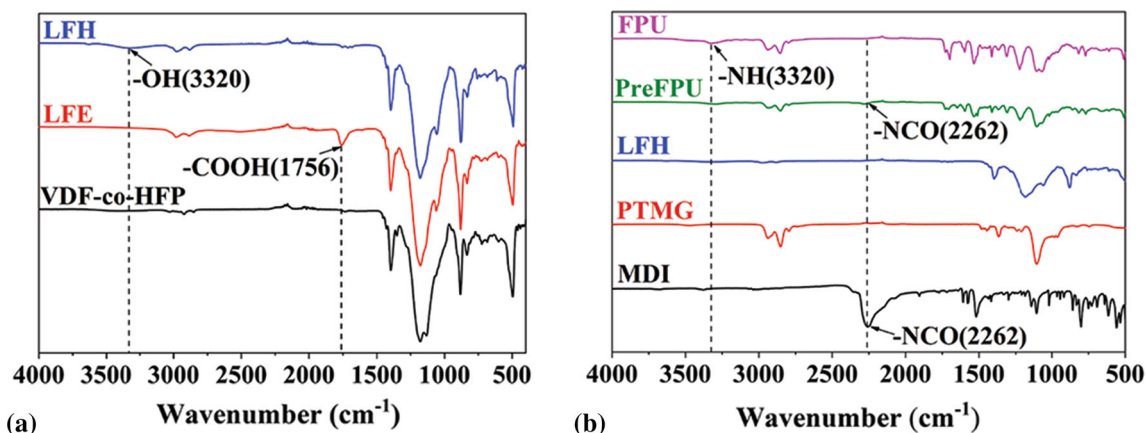
Fig. 2 ATR-FTIR spectra of the FPU and the relevant materials. (a), VDF-co-HFP, LFE and LFH; (b), MDI, PTMG, LFH, PreFPU and FPU

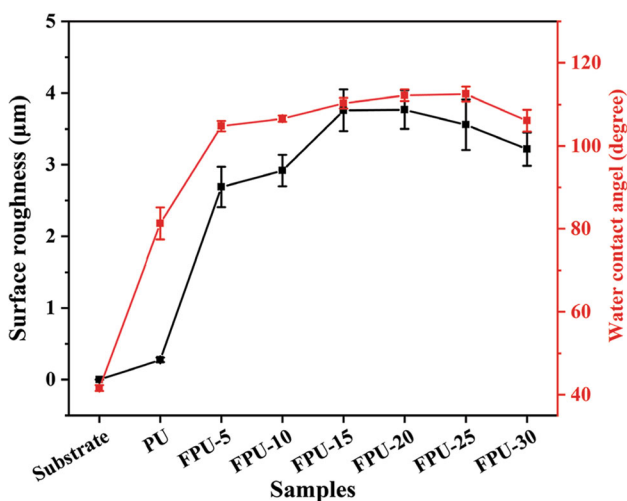**Fig. 3** Surface roughness and water contact angle of the substrate, the PU and the FPU with different dosages of LFH

Fig. 4 Water contact angle on the surface of SS-PU, SS-FPU, Al-PU and Al-FPU with different proportions of PU and FPU at room temperature

decrease, and the hydrophobic effect deteriorated. Surface enrichment is an important characteristic of FPU (Ref 38). With the introduction of the fluorine element, the fluorine-containing segment can migrate to the surface, and the particles can nucleate on the surface, growing into a protrusive and rough structure. When further increasing the LFH content, the rich fluorine content on the surface of the FPU will increase the nucleation rate. Thus, the number of the protrusive structures will increase, and the size will reduce (Ref 40, 41). Therefore, the surface of FPU was relatively smooth, and the roughness was reduced. This consequence indicates that the hydrophobic surface resulted from the synergy between surface energy and roughness. Hence, to achieve the best hydrophobicity, the dosage of LFH should be limited within 25 wt.%, and FPU-20 is the best choice in this study.

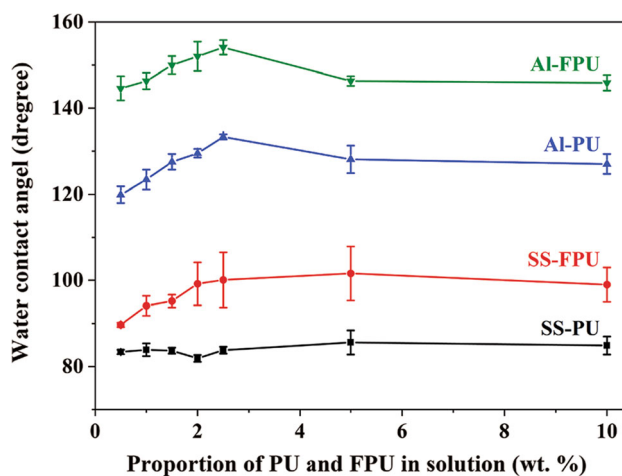To reveal the effects of the surface energy and roughness on hydrophobicity, the WCA of the 316L SS and the Al coatings (of which the surface roughness was different) modified with PU and FPU-20 (denoted as SS-PU/FPU for the 316L SS substrates modified by PU/FPU and Al-PU/FPU for the modified Al coatings, respectively) was investigated. The result indicates that the addition of PU/FPU effectively altered the hydrophobicity of the 316L SS substrates and the Al coatings (Fig. 4). As the proportion of PU increased, the WCA of the SS-PU surface did not exhibit a noticeable increase. However, compared with the SS-PU, the hydrophobicity of SS-FPU was improved significantly. When the proportion of FPU reached 2.5 wt.%, the WCA increased from 89.7±0.5° to 100.1±6.4°. This is because the introduction of the fluorine atoms reduced the surface energy of the coatings, resulting in increased hydrophobicity. However, the further increase in the proportion of FPU did not lead to a further increase in WCA.

The Al coatings appeared hydrophobic after the addition of PU, and the increase in the PU content correlated with the WCA of the coatings significantly. The WCA increased from 119.9±1.9° for the surface modified with 0.5 wt.%
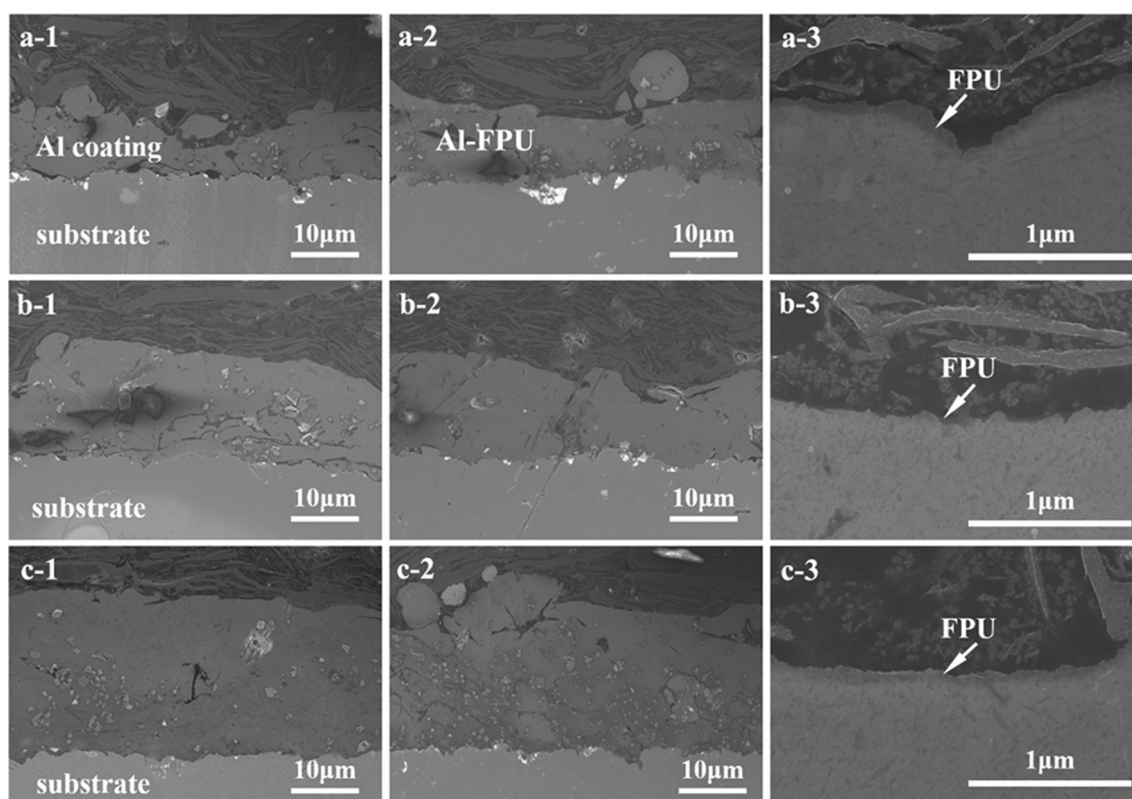
Fig. 5 Cross-sectional SEM images of the Al coatings (a-1, b-1 and c-1) and Al-FPU (a-2, b-2 and c-2) coatings of different thicknesses. a-3, b-3 and c-3 are images at high magnifications

Table 2 Water contact angles for Al-PU and Al-FPU coatings of different thicknesses

The thickness of Al coating, μm	Water contact angle, °	
	Al-PU	Al-FPU
20	114.9±1.7	138.5±1.6
40	129.3±1.2	143.9±1.9
70	136.3±2.2	153.6±2.0

PU to 133.3±0.6° for the surface modified with 2.5 wt.% PU. The increased WCA was attributed to the Al coatings providing a rough surface structure that led to the formation of hydrophobic surfaces. This indicates that an increase in roughness may be beneficial to improving surface hydrophobicity. Furthermore, the superhydrophobicity was achieved when the FPU content reached 1.5 wt.%, and the WCA reached a maximum of 154.1±1.7° when the surface comprised 2.5 wt.% FPU. However, the sliding angle of the water droplets was about 16.5°, which is attributed to the rough surface of the superhydrophobic coating, making the droplets less likely to slide. On the other hand, further increasing the proportion of PU and FPU did not lead to further improvement in WCA. This is

because when the PU and FPU concentrations reached a certain threshold, the thickness of their deposition on the Al coating could grow, and the original rough surface structure of the Al coating changed, resulting in a decrease in WCA. These results suggest that a superhydrophobic surface was achieved by the synergy between surface energy and surface roughness.

To study the effect of the thickness of the as-sprayed Al coating on the hydrophobic properties, three arc-sprayed Al coatings with different thicknesses were prepared and then soaked in PU or FPU solutions with a concentration of 2.5% to obtain Al-PU and Al-FPU coatings. Figure 5 presents a cross-sectional view of the Al coating and the Al-FPU coatings of different thicknesses, showing that the Al coatings were approximately 20 μm, 40 μm and 70 μm thick, respectively (Fig. 5a-1, b-1 and c-1). Furthermore, more porosity tended to occur in the thin Al coating (Fig. 5a-1), while the Al coatings became denser as the thickness increased (Fig. 5c-1). In addition, Fig. 5(a-2, b-2 and c-2) showed the cross-sectional view of the Al-FPU coating after soaking. Due to the short soaking time, the PU and the FPU layers were very thin (Fig. 5a-3, b-3 and c-3).

Table 2 shows the WCA of the Al-PU and the Al-FPU coatings with different Al thicknesses. When the thickness of the Al coating was about 20 μm, the WCA of the Al-PU
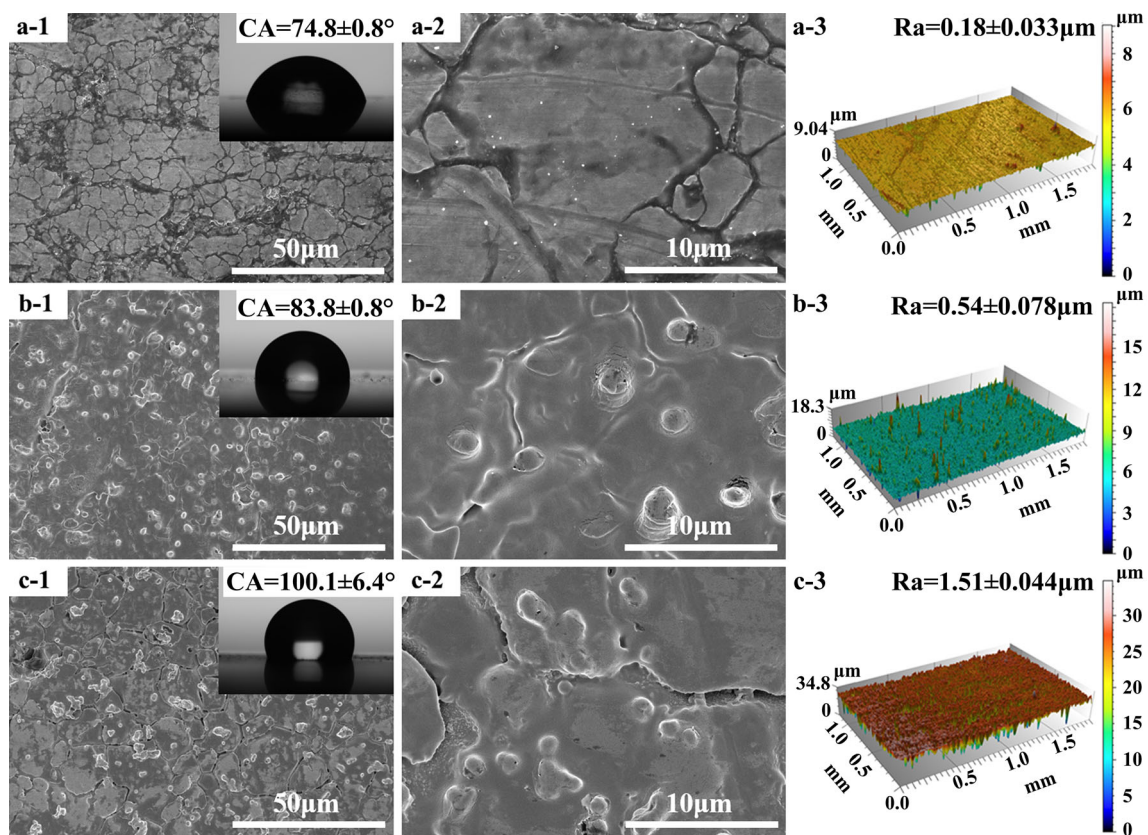
Fig. 6 Characterization of the SS-PU/FPU coatings. (a), 316L SS; (b), SS-PU; (c), SS-FPU; 1-2, SEM images at low and high magnification (Insets are the images of water droplet placed on the samples); 3, surface profiles

coating was 114.9±1.7°. Even if the fluorine was introduced, the obtained Al-FPU coating could not achieve superhydrophobicity, and the WCA was 138.5±1.6°. As the thickness of the Al coating increased to about 70 μm, the WCA of the Al-PU coating reached 136.3±2.2°, and the water repellency was significantly improved. Furthermore, the Al-FPU coating reached superhydrophobic (153.6±2.0°) due to the introduction of fluorine with LSE. The results show that the thickness of the Al coating had a great impact on the wetting properties of the coating. Meanwhile, an appropriate thickness can not only improve the water resistance but also densify the structure of the coating.

The surface morphologies, surface wettability and surface roughness of the untreated 316L SS substrate and the Al coatings with a concentration of 2.5 wt.% PU/FPU were further characterized by SEM, WCA measurements and 3D optical profilometer (Fig. 6). For the untreated 316L SS, the surface was flat, but had some cracks, and the WCA was about 74.8±0.8° (Fig. 6a-1 and a-2). The R_a of the substrate was about 0.18 μm (Fig. 6a-3). After modification with an extremely thin PU/FPU layer, the 316L SS had relatively rough surfaces with nubble protrusion (Fig. 6b and c). For SS-PU, the surface exhibited hydrophobicity with a WCA of about 83.8±0.8° (inset in Fig. 6b-1), and

the R_a of the coating was about 0.54 μm (Fig. 6b-3). For SS-FPU, the surface showed better hydrophobicity with a WCA of about 100.1±6.4° (inset in Fig. 6c-1), and the R_a of the coating was about 1.51 μm (Fig. 6c-3). For 316L SS with low roughness, the hydrophobicity can be effectively improved with the addition of the 2.5 wt.% FPU.

For the arc-sprayed Al coatings, the surface showed a relatively high R_a of about 12.32 μm (Fig. 7a-3), showing exceedingly hydrophilic on the surface with WCA of about 17.8±1.6° (inset in Fig. 7a-3). After modification with an extremely thin PU/FPU layer, many nubble protrusions appeared on the surfaces (Fig. 7b-1, b-2, c-1 and c-2). The R_a values of the Al-PU and the Al-FPU coatings were about 9.85 μm and 8.94 μm, respectively (Fig. 7b-3 and c-3). It is noted that the PU/FPU-modified Al coatings showed lower R_a compared with the as-sprayed Al coating, possibly due to the PU/FPU filling-in to the preexisting defects of the Al coating. The WCA test shows the WCA of Al-PU coating was about 133.3±0.6° (inset in Fig. 7b-1), whose hydrophobicity was much better than that of SS-PU (inset in Fig. 6b-1). The results indicate that a rough structure was beneficial in improving surface hydrophobicity. Furthermore, with the introduction of fluorine atoms, the surface of the Al-FPU coating presented superhydrophobicity with a WCA of about 154.1±1.7°.
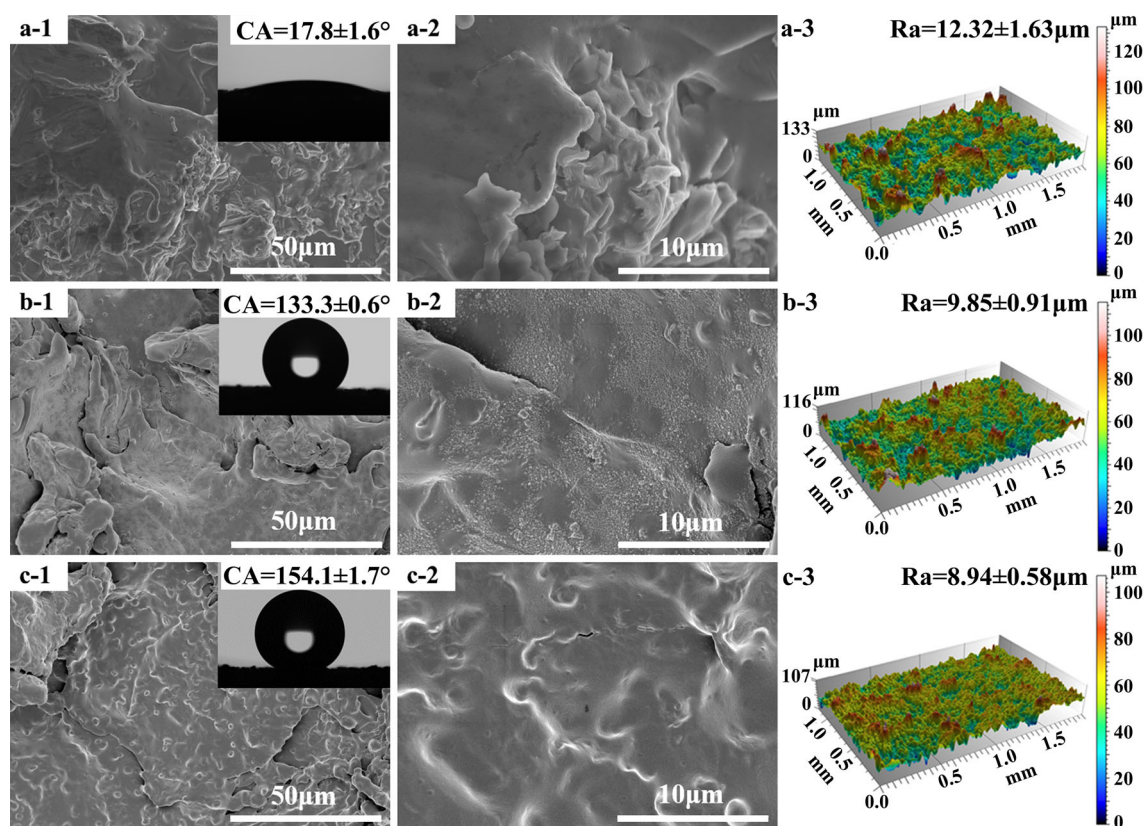
Fig. 7 Characterization of the Al-PU/FPU coatings. (a), Al coating; (b), Al-PU; (c), Al-FPU; 1-2, SEM images at low and high magnification (the reduced photographs show the WCA); 3, surface profiles
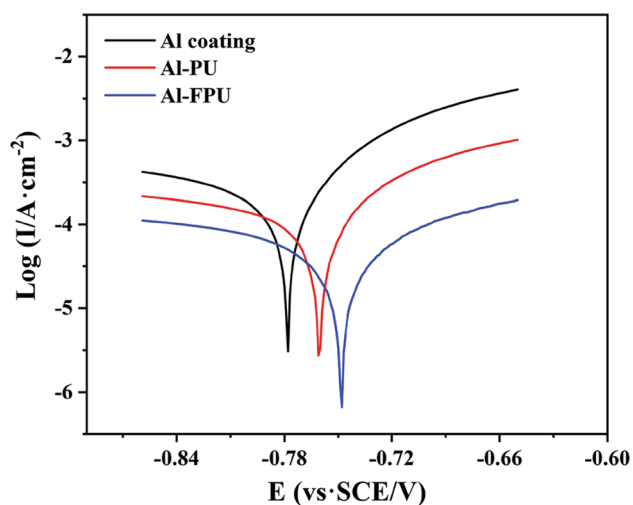

Fig. 8 Potentiodynamic polarization curves of the Al coating, Al-PU coating and Al-FPU coating tested in artificial seawater

Nonetheless, the WCA decreased with the increase in the proportion of PU/FPU in the solution (Fig. 4). This may result from a higher concentration of PU/FPU that covered the island structures, reducing the contribution of the rough structure to superhydrophobicity. It is worth noting that the

WCA of pure FPU-20 film surface was $112.2\pm1.4°$ (Fig. 3), much lower than the WCA of Al-FPU coating. This result suggests that the superhydrophobicity of Al-FPU coating was ascribed to the synergy of the FPU with LSE and the Al coating with a rough surface. Apart from the LSE, it is considered that surface roughness also plays an essential role in achieving superhydrophobicity (Ref 42). Furthermore, the arc-sprayed Al coatings may have some preexisting defects, and thus, the solution of PU/FPU can spread easily and cure the pores or microcracks inside the Al coating, which may improve their corrosion resistance.

The corrosion resistance of the superhydrophobic coatings prepared in this work was investigated via Tafel polarization curves and electrochemical impedance spectra in artificial seawater (ASW) at 25 °C. The potentiodynamic polarization curves of the Al coating, Al-PU coating and Al-FPU coating in ASW are plotted in Fig. 8, and the values of corrosion potentials (E_{corr}) and corrosion current densities (I_{corr}) were recorded by electrochemical analytical software (Table 3). The E_{corr} and I_{corr} values of the Al coating were -0.778 V and 9.058×10^{-4} A·cm^{-2}, respectively. After the modification with PU/FPU, the values of E_{corr} for the Al-PU and the Al-FPU coatings were -0.761 and -0.748 V, respectively, which were higher than that of

Table 3 Results for electrochemical impedance spectroscopy (EIS), corrosion potentials (E_{corr}) and corrosion current densities (I_{corr}) of the coatings in artificial seawater

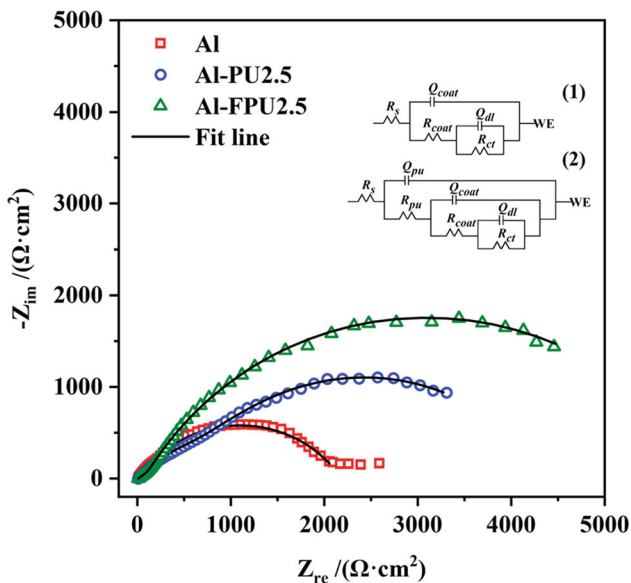| Parameters	Al coating	Al-PU coating	Al-FPU coating
R_s, $\Omega \cdot cm^2$	7.023	5.932	6.585
Q_{pu}, $\mu F \cdot cm^{-2} \cdot s^{n-1}$	…	53.50	81.79
R_{pu}, $\Omega \cdot cm^2$	…	102.8	210.1
n_1	…	0.74	0.63
Q_{coat}, $\mu F \cdot cm^{-2} \cdot s^{n-1}$	545.3	186.0	145.5
R_{coat}, $\Omega \cdot cm^2$	442.8	968.6	146.2
n_2	0.62	0.64	0.63
Q_{dl}, $\mu F \cdot cm^{-2} \cdot s^{n-1}$	279.9	711.8	279.4
R_{ct}, $\Omega \cdot cm^2$	5467	3285	5963
n_3	0.85	0.67	0.70
χ^2, $\times 10^{-3}$	1.74	0.25	0.36
E_{corr}, V	−0.778	−0.761	−0.748
I_{corr}, $A \cdot cm^{-2}$	9.058×10^{-4}	1.235×10^{-4}	1.238×10^{-4}

Fig. 9 Nyquist plots of the coatings and the equivalent circuit models. 1, the equivalent circuit models of Al coating; 2, Al-PU/FPU coatings. R_s: solution resistance; Q_{coat}: capacitance of Al coating; R_{coat}: resistance of Al coating; Q_{dl}: capacitance of the double layer; R_{ct}: charge transfer resistance; Q_{pu}: capacitance of PU/FPU layer; R_{pu}: resistance of PU/FPU layer

the Al coating. The corrosion potential provides information about the corrosion tendency of the samples, showing that the corrosion resistance is positively correlated with the corrosion potential (Ref 43). Besides, the I_{corr} values of the Al-PU and the Al-FPU coatings were 1.235×10^{-4} and 1.238×10^{-4} A·cm^{-2}, respectively. It is worth noting that the corrosion current density of the Al-FPU coating with superhydrophobic surfaces was much lower than that of the Al coating. It is believed that the lower corrosion current density and the higher corrosion potential suggesting a lower corrosion rate and better corrosion resistance, which is consistent with the results reported in previous studies

(Ref 35, 44). The good corrosion resistance of the Al-FPU is due to densified micromorphology of the Al coating after being deposited by the PU/FPU (Fig. 6), which also sealed the pores in the Al coating. In addition, the water repellent effect of the superhydrophobic surface can effectively inhibit the migration and penetration of corrosive media into the Al coating, thereby improving the corrosion resistance. Therefore, the Al-FPU coating with superhydrophobic surfaces exhibited better corrosion resistance than other coatings previously discussed in this study, indicating that it can resist corrosion effectively.

Figure 9 illustrates the Nyquist plots and the equivalent circuit models for the Al, the Al-PU and the Al-FPU coatings in ASW. The Nyquist plots of the coatings indicate that the diameter of the capacitive arc for the Al-PU and the Al-FPU coatings was greater than that for the Al coating. In general, a large diameter of the capacitive arc suggests a better barrier property (Ref 45). The result shows that the corrosion resistance of the coating was enhanced remarkably after FPU treatment, which was in accordance with the potentiodynamic polarization curve (Fig. 8). The equivalent circuit was attained by ZSimpWin software as shown in Fig. 9 (diagram 1 and 2). It consisted of R_s, Q_{pu}, R_{pu}, Q_{coat}, R_{coat}, Q_{dl} and R_{ct}, which denoted the solution resistance, the capacitance of PU/FPU layer, the resistance of PU/FPU layer, the capacitance of Al coating, the resistance of Al coating, the capacitance of the double layer and the charge transfer resistance, respectively. The results show that the R(R(R(QR))) model was suitable for the Al coating, which was consistent with previous studies (Ref 46, 47). However, after the soaking treatment of the Al coating, the surface was protected by a layer of PU/FPU, preventing the coating from the penetration of the electrolyte. Hence, the R(Q(R(Q(R(QR))))) model was appropriate for the Al-PU coating and Al-FPU coating. The fitted results for electrochemical impedance spectroscopy

Fig. 10 Photographs of the surface of the samples before and after the neutral salt spray test. a-1, b-1, c-1 and d-1 are digital photographs of the pretested 316L SS, Al coating, Al-PU coating and Al-FPU coating, and a-2, b-2, c-2 and d-2 are digital photographs of the posttested 316L SS, Al coating, Al-PU coating and Al-FPU coating
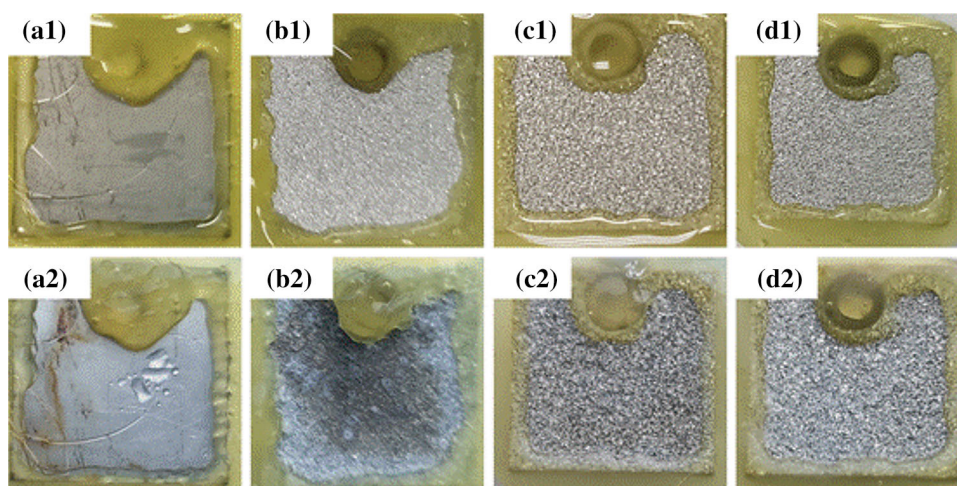
(EIS) of the coatings are summarized in Table 3. The R_{pu} and R_{ct} values of the Al-FPU coating were 210.1 $\Omega \cdot cm^2$ and 5963 $\Omega \cdot cm^2$, respectively, which were higher than those of the Al-PU coating (102.8^2 and 3285 $\Omega \cdot cm^2$, respectively). This suggests that the corrosion resistance of the coatings with superhydrophobic surfaces was enhanced, which agreed with the analytical results of the potentiodynamic polarization curve (Fig. 8). Arc-sprayed Al coatings have relatively good corrosion resistance, but in long-term use, the preexisting defects on the surface may result in poor durability. The microstructure morphology of the coating has shown that the addition of FPU layer provided a more densified appearance of the coating. The superhydrophobic layer could effectively inhibit the migration of corrosive ions into the Al coating, thereby improving the corrosion resistance of the coating (Ref 35). Meanwhile, air may be trapped in the grooves on the rough superhydrophobic surface, minimizing the contact area between the corrosive media and the FPU layer and becoming a barrier that significantly hinders the corrosion of metal and alloy surfaces (Ref 48).

Figure 10 shows the photographs of the samples after the salt spray test, which reveals the long-term corrosion resistance of the samples. Before the salt spray test, the substrate and the coating surfaces were intact (Fig. 10a-1, b-1, c-1 and d-1). After the 360h salt spray test, corrosion sites appeared on the surface of 316L SS (Fig. 10a-2), and the Al coating darkened significantly with the formation of many bubbles and some corrosion pits (Fig. 10b-2). The surface of the Al-PU coating showed many black corrosion spots (Fig. 10c-2), but the coating was almost intact, as the PU had filled the pores in the coating and effectively blocked the contact between corrosive media and the coating. The Al-FPU coating had no obvious surface change before and after the test (Fig. 10d-2), as the

superhydrophobic effect of Al-FPU composite coating can further prevent the contact between the corrosive media and the coating, thus improving the corrosion resistance of the coating.

Conclusions

In summary, PU and FPU were successfully synthesized via the designed routes using VDF-co-HFP, MDI, LFH and PTMG. A superhydrophobic coating of FPU was formed on the arc-sprayed Al coating, and the FPU modified coatings showed resistance to corrosion. The following conclusions can be drawn:

(1) Fluorine was successfully introduced to PU as per the designed routes, forming FPU.

(2) Increasing the fluorine content in FPU could improve the hydrophobicity at a low fluorine content, but decrease when the content was high.

(3) Increasing the concentration of the PU/FPU in the coatings could enhance the hydrophobicity when the concentration was low, but compromise when the concentration was high.

(4) The thickness of the as-sprayed Al coating could affect the hydrophobicity of the Al-PU/FPU coatings.

(5) The FPU coating (when the concentration was 2.5 wt.%) formed on a rough Al surface was superhydrophobic and had good resistance to corrosion.

Reference

1. A.M.A. Mohamed, A.M. Abdullah, and N.A. Younan, Corrosion Behavior of Superhydrophobic Surfaces: A Review, *Arab. J. Chem.*, 2015, **8**(6), pp. 749-765. https://doi.org/10.1016/j.arabjc.2014.03.006

2. M. Ma and R.M. Hill, Superhydrophobic Surfaces, *Curr. Opin. Colloid Interface Sci.*, 2006, **11**(4), pp. 193-202. https://doi.org/10.1016/j.cocis.2006.06.002

3. X. Zhang, F. Shi, J. Niu, Y. Jiang, and Z. Wang, Superhydrophobic Surfaces: From Structural Control to Functional Application, *J. Mater. Chem.*, 2008, **18**(6), pp. 621-633. https://doi.org/10.1039/b711226b

4. S.S. Latthe, C. Terashima, K. Nakata, M. Sakai, and A. Fujishima, Development of Sol-Gel Processed Semi-Transparent and Self-Cleaning Superhydrophobic Coatings, *J. Mater. Chem. A*, 2014, **2**(15), pp. 5548-5553. https://doi.org/10.1039/c3ta15017h

5. A. Nakajima, K. Hashimoto, T. Watanabe, K. Takai, G. Yamauchi, and A. Fujishima, Transparent Superhydrophobic Thin Films with Self-Cleaning Properties, *Langmuir*, 2000, **16**(17), pp. 7044-7047. https://doi.org/10.1021/la000155k

6. I. Banerjee, R.C. Pangule, and R.S. Kane, Antifouling Coatings: Recent Developments in the Design of Surfaces That Prevent Fouling by Proteins, Bacteria, and Marine Organisms, *Adv. Mater.*, 2011, **23**(6), pp. 690-718. https://doi.org/10.1002/adma.201001215

7. Y. Wei, L. Hongtao, and Z. Wei, Preparation of Anti-Corrosion Superhydrophobic Coatings by an Fe-Based Micro/Nano Composite Electro-Brush Plating and Blackening Process, *RSC Adv.*, 2015, **5**(125), pp. 103000-103012. https://doi.org/10.1039/c5ra15640h

8. L. Cao, A.K. Jones, V.K. Sikka, J. Wu, and D. Gao, Anti-Icing Superhydrophobic Coatings, *Langmuir*, 2009, **25**(21), pp. 12444-12448. https://doi.org/10.1021/la902882b

9. S. Farhadi, M. Farzaneh, and S.A. Kulinich, Anti-Icing Performance of Superhydrophobic Surfaces, *Appl. Surf. Sci.*, 2011, **257**(14), pp. 6264-6269. https://doi.org/10.1016/j.apsusc.2011.02.057

10. M. Zhai, Y. Gong, X. Chen, T. Xiao, G. Zhang, L. Xu, and H. Li, Mass-Producible Hydrophobic Perfluoroalkoxy/Nano-Silver Coatings by Suspension Flame Spraying for Antifouling and Drag Reduction Applications, *Surf. Coat. Technol.*, 2017, **328**, pp. 115-120. https://doi.org/10.1016/j.surfcoat.2017.08.049

11. T. Nishino, M. Meguro, K. Nakamae, M. Matsushita, and Y. Ueda, The Lowest Surface Free Energy Based on -Cf3 Alignment, *Langmuir*, 1999, **15**(13), pp. 4321-4323. https://doi.org/10.1021/la981727s

12. S. Das, S. Kumar, S.K. Samal, S. Mohanty, and S.K. Nayak, A Review on Superhydrophobic Polymer Nanocoatings: Recent Development, Application, *Ind. Eng. Chem. Res.*, 2018, **57**(8), pp. 2727-2745. https://doi.org/10.1021/acs.iecr.7b04887

13. S. Li, P. Li, Y. Tian, and Y. Zheng, Fluffy Polyfluoroalkoxy Layer Produced by Air Plasma Spraying Based on "Grapeshot" Effect, *J. Therm. Spray Technol.*, 2019, **29**(3), pp. 462-470. https://doi.org/10.1007/s11666-019-00965-y

14. A. Fihri, E. Bovero, A. Al-Shahrani, A. Al-Ghamdi, and G. Alabedi, Recent Progress in Superhydrophobic Coatings Used for Steel Protection: A Review, *Colloids Surf. A*, 2017, **520**, pp. 378-390. https://doi.org/10.1016/j.colsurfa.2016.12.057

15. S.D. Bhagat, Y.-H. Kim, and Y.-S. Ahn, Room Temperature Synthesis of Water Repellent Silica Coatings by the Dip Coat Technique, *Appl. Surf. Sci.*, 2006, **253**, pp. 2217-2221. https://doi.org/10.1016/j.apsusc.2006.04.030

16. H. Zheng, M. Pan, J.Y. Jie Wen, L. Zhu, and H. Yu, Robust, Transparent and Superhydrophobic Coating Fabricated with Waterborne Polyurethane and Inorganic Nanoparticle Composites, *Ind. Eng. Chem. Res.*, 2019, **58**(19), pp. 8050-8060. https://doi.org/10.1021/acs.iecr.9b00052

17. C. Jeong and C.H. Choi, Single-Step Direct Fabrication of Pillar-on-Pore Hybrid Nanostructures in Anodizing Aluminum for Superior Superhydrophobic Efficiency, *ACS Appl. Mater. Interfaces*, 2012, **4**(2), pp. 842-848. https://doi.org/10.1021/am201514n

18. F. Shi, Z. Wang, and X. Zhang, Combining a Layer-by-Layer Assembling Technique with Electrochemical Deposition of Gold Aggregates to Mimic the Legs of Water Striders, *Adv. Mater.*, 2005, **17**(8), pp. 1005-1009. https://doi.org/10.1002/adma.200402090

19. J. Feng, M.T. Tuominen, and J.P. Rothstein, Hierarchical Superhydrophobic Surfaces Fabricated by Dual-Scale Electron-Beam-Lithography with Well-Ordered Secondary Nanostructures, *Adv. Funct. Mater.*, 2011, **21**(19), pp. 3715-3722. https://doi.org/10.1002/adfm.201100665

20. S.A. Mahadik, M.S. Kavale, S.K. Mukherjee, and A.V. Rao, Transparent Superhydrophobic Silica Coatings on Glass by Sol-Gel Method, *Appl. Surf. Sci.*, 2010, **257**(2), pp. 333-339. https://doi.org/10.1016/j.apsusc.2010.06.062

21. M. Ma, Y. Mao, M. Gupta, K.K. Gleason, and G.C. Rutledge, Superhydrophobic Fabrics Produced by Electrospinning and Chemical Vapor Deposition, *Macromolecules*, 2005, **38**(23), pp. 9742-9748. https://doi.org/10.1021/ma0511189

22. S. Wang, Y. Li, X. Fei, M. Sun, C. Zhang, Y. Li, Q. Yang, and X. Hong, Preparation of a Durable Superhydrophobic Membrane by Electrospinning Poly (Vinylidene Fluoride) (Pvdf) Mixed with Epoxy-Siloxane Modified Sio2 Nanoparticles: A Possible Route to Superhydrophobic Surfaces with Low Water Sliding Angle and High Water Contact Angle, *J. Colloid Interf. Sci.*, 2011, **359**(2), pp. 380-388. https://doi.org/10.1016/j.jcis.2011.04.004

23. E. Bormashenko, S. Balter, Y. Bormashenko, and D. Aurbach, Honeycomb Structures Obtained with Breath Figures Self-Assembly Allow Water/Oil Separation, *Colloids Surf. A*, 2012, **415**, pp. 394-398. https://doi.org/10.1016/j.colsurfa.2012.09.022

24. K.P. Fischer, W.H. Thomason, T. Rosbrook, and J. Murali, Performance History of Thermal-Sprayed Aluminum Coatings in Offshore Service, *Mater. Perform.*, 1995, **34**(4), pp. 27-35.

25. D. Chaliampalias, G. Vourlias, E. Pavlidou, G. Stergioudis, S. Skolianos, and K. Chrissafis, High Temperature Oxidation and Corrosion in Marine Environments of Thermal Spray Deposited Coatings, *Appl. Surf. Sci.*, 2008, **255**, pp. 3104-3111. https://doi.org/10.1016/j.apsusc.2008.08.101

26. A. Pardo, P. Casaju, M. Mohedano, A.E. Coy, F. Viejo, B. Torres, and E. Matykina, Corrosion Protection of Mg/Al Alloys by Thermal Sprayed Aluminium Coatings, *Appl. Surf. Sci.*, 2009, **255**, pp. 6968-6977. https://doi.org/10.1016/j.apsusc.2009.03.022

27. S.A. Galedari, A. Mahdavi, F. Azarmi, Y. Huang, and A. McDonald, A Comprehensive Review of Corrosion Resistance of Thermally-Sprayed and Thermally-Diffused Protective Coatings on Steel Structures, *J. Therm. Spray Techn.*, 2019, **28**, pp. 645-677. https://doi.org/10.1007/s11666-019-00855-3

28. M. Campo, M. Carboneras, M.D. López, B. Torres, P. Rodrigo, E. Otero, and J. Rams, Corrosion Resistance of Thermally Sprayed Al and Al/Sic Coatings on Mg, *Surf. Coat. Techn.*, 2009, **203**(20–21), pp. 3224-3230. https://doi.org/10.1016/j.surfcoat.2009.03.057

29. B. Wielage, U. Hofmann, S. Steinhauser, and G. Zimmermann, Improving Wear and Corrosion Resistance of Thermal Sprayed Coatings, *Surf. Eng.*, 1998, **14**(2), pp. 136-138.

30. E. Lugscheider, P. Jakiel, V. Messerschmidt, and G. Beckschulte, Subsequent Sealing of Thermally Sprayed Coatings to Increase Corrosion Resistance, *Surf. Eng.*, 1994, **10**(1), pp. 46-51. https://doi.org/10.1179/sur.1994.10.1.46

31. J. Knuuttila, P. Sorsa, and T. Mäntylä, Sealing of Thermal Spray Coatings by Impregnation, *J. Therm. Spray Techn.*, 1999, **8**(2), pp. 249-257. https://doi.org/10.1007/s11666-999-0002-2

32. M.P. Kanouff, R.A. Neiser, and T.J. Roemer, Surface Roughness of Thermal Spray Coatings Made with Off-normal Spray Angles, *J. Therm. Spray Tech.*, 1998, **7**, pp. 219-228. https://doi.org/10.1361/105996398770350963

33. D. Tejero-Martin, M.R. Rad, A. McDonald, and T. Hussain, Beyond Traditional Coatings: A Review on Thermal-Sprayed Functional and Smart Coatings, *J. Therm. Spray Tech.*, 2019, **28**, pp. 598-644. https://doi.org/10.1007/s11666-019-00857-1

34. X. Chen, Y. Gong, X. Suo, J. Huang, Y. Liu, and H. Li, Construction of Mechanically Durable Superhydrophobic Surfaces by Thermal Spray Deposition and Further Surface Modification, *Appl. Surf. Sci.*, 2015, **356**, pp. 639-644. https://doi.org/10.1016/j.apsusc.2015.08.156

35. X. Chen, J. Yuan, J. Huang, K. Ren, Y. Liu, S. Lu, and H. Li, Large-Scale Fabrication of Superhydrophobic Polyurethane/Nano-Al$_2$O$_3$ Coatings by Suspension Flame Spraying for Anti-Corrosion Applications, *Appl. Surf. Sci.*, 2014, **311**, pp. 864-869. https://doi.org/10.1016/j.apsusc.2014.05.186

36. D. Li and M. Liao, Dehydrofluorination Mechanism, Structure and Thermal Stability of Pure Fluoroelastomer (Poly(VDF-ter-HFP-ter-TFE) Terpolymer) in Alkaline Environment, *J. Fluorine Chem.*, 2017, **201**, pp. 55-67. https://doi.org/10.1016/j.jfluchem.2017.08.002

37. J. Li, Y. Lu, Y. Liu, Y. Li, X. Zhang, and S. Qi, Synthesis, Characterization, Curing and Properties of Carboxyl-Terminated Liquid Fluoropolymers, *Polym-Plast. Tech. Eng.*, 2014, **53**(1), pp. 46-53. https://doi.org/10.1080/03602559.2013.843688

38. N. Li, F.L. Zeng, Y. Wang, D. Qu, W. Hu, Y. Luan, S. Dong, J. Zhang, and Y. Bai, Fluorinated Polyurethane Based on Liquid Fluorine Elastomer (LFE) Synthesis via Two-Step Method: The Critical Value of Thermal Resistance and Mechanical Properties, *RSC Adv.*, 2017, **7**(49), pp. 30970-30978. https://doi.org/10.1039/c7ra04509c

39. H. Yang, M. Zhang, R. Chen, Q. Liu, J. Liu, J. Yu, H. Zhang, P. Liu, C. Lin, and J. Wang, Polyurethane Coating with Heterogeneity Structure Induced by Microphase Separation: A New Combination of Antifouling and Cavitation Erosion Resistance, *Prog. Org. Coat.*, 2021, **151**, pp. 106032. https://doi.org/10.1016/j.porgcoat.2020.106032

40. U. Cengiz and H.Y. Erbil, Superhydrophobic Perfluoropolymer Surfaces Having Heterogeneous Roughness Created by Dip-Coating from Solutions Containing a Nonsolvent, *Appl. Surf. Sci.*, 2014, **292**, pp. 591-597. https://doi.org/10.1016/j.apsusc.2013.12.013

41. J. Wang, A. Raza, Y. Si, L. Cui, J. Ge, B. Ding, and J. Yu, Synthesis of Superamphiphobic Breathable Membranes Utilizing SiO$_2$ Nanoparticles Decorated Fluorinated Polyurethane Nanofibers, *Nanoscale*, 2014, **4**, pp. 7549-7556. https://doi.org/10.1039/C2NR32883F

42. S. Shibuichi, T. Onda, N. Satoh, and K. Tsujii, Super Water-Repellent Surfaces Resulting from Fractal Structure, *J. Phys. Chem.*, 1996, **100**(50), pp. 19512-19517. https://doi.org/10.1021/jp9616728

43. E.C. Gomes and M.A.S. Oliveira, Corrosion Protection by Multilayer Coating Using Layer-by-Layer Technique, *Surf. Coat. Technol.*, 2011, **205**(8-9), pp. 2857-2864. https://doi.org/10.1016/j.surfcoat.2010.10.061

44. J. Wang, D. Li, Q. Liu, X. Yin, Y. Zhang, X. Jing, and M. Zhang, Fabrication of Hydrophobic Surface with Hierarchical Structure on Mg Alloy and Its Corrosion Resistance, *Electrochim. Acta*, 2010, **55**(22), pp. 6897-6906. https://doi.org/10.1016/j.electacta.2010.05.070

45. F. Sun, S. Ren, Z. Li, Z. Liu, X. Li, and C. Du, Comparative Study on the Stress Corrosion Cracking of X70 Pipeline Steel in Simulated Shallow and Deep Sea Environments, *Mater. Sci. Eng. A*, 2017, **685**, pp. 145-153. https://doi.org/10.1016/j.msea.2016.12.118

46. Y. Tian, H. Zhang, X. Chen, A. McDonald, S. Wu, T. Xiao, and H. Li, Effect of Cavitation on Corrosion Behavior of HVOF-Sprayed WC-10Co4Cr Coating with Post-Sealing in Artificial Seawater, *Surf. Coat. Technol.*, 2020, **397**, pp. 126012. https://doi.org/10.1016/j.surfcoat.2020.126012

47. X. Wang, H. Zhao, S. Wu, X. Suo, X. Wei, and H. Li, Aluminum-Polyethylene Composite Coatings with Self-Sealing Induced Anti-Corrosion Performances, *J. Mater. Process. Technol.*, 2020, **282**, pp. 116642. https://doi.org/10.1016/j.jmatprotec.2020.116642

48. P. Bi, H. Li, G. Zhao, M. Ran, L. Cao, H. Guo, and Y. Xue, Robust Super-Hydrophobic Coating Prepared by Electrochemical Surface Engineering for Corrosion Protection, *Coatings*, 2019, **9**(7), pp. 452-470. https://doi.org/10.3390/coatings9070452